TURBULENT HEAT TRANSFER FOR IMPINGING JET FLOWING INSIDE A CYLINDRICAL HOT CAVITY

by

Yacine HALOUANE [a], ***Amina MATAOUI*** [b*], ***and Farida IACHACHENE*** [b]

[a] Department for Energy, Faculty of Engineering Sciences, UMBB, Boumerdes, Algeria
[b] Laboratory for Theoretical and Applied Fluid Mechanics, Faculty of Physics, University of Sciences and Technology Houari Boumediene, Alger, Algeria

Original scientific paper
DOI: 10.2298/TSCI121001092H

Convective heat transfer from an isothermal hot cylindrical cavity due to a turbulent round jet impingement is investigated numerically. Three-dimensional turbulent flow is considered in this work. The Reynolds stress second order turbulence model with wall standard treatment is used for the turbulence predictions the problem parameters are the jet exit Reynolds number, ranging from $2\cdot10^4$ to 10^5 and the normalized impinging distance to the cavity bottom and the jet exit L_f, ranging from 4 to 35. The computed flow patterns and isotherms for various combinations of these parameters are analyzed in order to understand the effect of the cavity confinement on the heat transfer phenomena. The flow in the cavity is divided into three parts, the area of free jet, and the area of the jet interaction with the reverse flow and the semi-quiescent flow in the region of the cavity bottom. The distribution of the local and mean Nusselt numbers along the cavity walls for above combinations of the flow parameters are detailed. Results are compared against to corresponding cases for impinging jet on a plate for the case of the bottom wall. The analysis reveals that the average Nusselt number increases considerably with the jet exit Reynolds number. Finally, it was found that the average Nusselt number at the stagnation point could be correlated by a relationship in the form $\overline{\mathrm{Nu}} = f(L_f, \mathrm{Re})$.

Key words: *round jet, cylindrical cavity, turbulence, thermal effect, finite volume method, Nusselt number*

Introduction

Impingement flows are extensively used for heating, cooling, and drying processes in different industrial applications. Impinging jets are used in paper and textile industries, the thermal treatment of materials, cooling of electronic components and turbine blades, and drying of continuous sheets of materials, *etc*. Some applications of dehydration by impinging jets are included in manufacturing of printed wiring boards, production of foodstuffs, de-icing of aircraft wings, annealing of metal sheets, tempering of glass, *etc*.

Although, numerous studies were conducted for jets impingement, it remains an active domain of research. Polat *et al*. [1] published a comprehensive review on the numerical analysis of impinging jet flow and heat transfer before 1989.

* Corresponding author; e-mail: mataoui_amina@yahoo.fr

Impinging jets onto a cavity are extremely complex flow configurations, where several interactions can occur on many surfaces simultaneously. Analysis of turbulent jet impingement on cavity is characterized by strong streamline curvature, entrainment, flow recirculation, pressure gradient, and boundary layer development on several impingement surfaces. Relatively few studies that have reported on the flow field and heat transfer characteristics due to an impinging jet with a cavity even though there are many engineering applications of such flow and heat transfer process.

This configuration was usually used in many industrial devices. It can simulate the ventilation of mines, the injection of fuel into the combustion chambers. There are many works published on this subject where the effect of the cavity shape and the jet location were examined. Gilard and Brizzi [2, 3] studied experimentally the behavior of a plane jet of thickness *d*, flowing into a cylindrical cavity provided with a hemispherical bottom. They used for the visualization and the measurements of the flow fields, the PIV technique. Choi *et al.* [4] present an experimental study of fluid flow and heat transfer of cooling by an impinging jet onto a semi-circular concave surface. The distributions of the mean velocity and fluctuations were measured within the free jet region, the impinging region and the wall jet flow region by using laser Doppler anemometer (LDV) technique. Local Nusselt numbers have also been computed in this work.

Shuja *et al*. [5-7] studied a flow exiting from a combination of conical and annular nozzles impinging a hot cylindrical cavity. They have examined the effects of the external angle of annular nozzle and the jet exit velocity on the flow interaction. The heat transfer and skin friction coefficients within a conical cavity are also illustrated in another study of these authors, where they presented the effect of nozzle shape, cavity diameter, and cavity depth, on the flow structure and heat transfer rates. Terekhov *et al*. [8] studied experimentally the heat transfer and the flow field generated by a turbulent jet impinging a spherical cavity. Colucci and Viskanta [9] considered the effects produced by a hyperbolic nozzle of a confined impinging air jet on the local heat transfer coefficient by thermo chromatic liquid-crystal technique. Jeng and Tzeng [10] investigated numerically an impinging confined slot jet for the cooling of porous metallic foam heat sink. Mataoui *et al*. [11, 12] have investigated experimentally and numerically using two scales turbulence model the case of a turbulent plane jet flowing into a rectangular cavity. The effect of the jet unsteadiness was detailed depending on the jet location inside the cavity. Jaramillo *et al*. [13] have tested numerically the case of a confined plane jet impinging a flat plate. They used the results obtained by a direct numerical simulation DNS of previous study to improve the performance of several Reynolds-averaged Navier-Stokes (RANS) models. Lawson *et al*. [14] have presented a technique for the control of the jet oscillation in a thin rectangular cavity, by subjecting perpendicularly another jet to the main jet through the lateral cavity wall. This study was conducted experimentally and numerically by 2-D and 3-D simulation. Schwarzer *et al*. [15] have made a combined experimental and numerical study of a turbulent round jet submerged in a rectangular cavity. Kang and Tao [16] have studied experimentally the heat and mass transfer of an axisymmetric jet impinging a cylindrical cavity with one end open to the ambient flow for the jet Reynolds number range of 10^4 to $8 \cdot 10^4$, and the dimensionless impinging distance between the jet exit and the cavity bottom *S/d* range from 1 to 4.5. Risso and Fabre [17] carried out an experimental study of an hydrodynamic jet confined in a vertical cylindrical cavity, open in its upper part. Baydar and Ozmen [18] conducted an experimental and numerical study for deepen the flow of a confined jet impinging perpendicularly the upper surface of the cavity. The mean velocity, turbulence intensity and pressure distributions in the stagnation zone were determined for Reynolds numbers ranging from 30,000 to 50,000 and for the dimensionless impinging distance between 0.2 and 6. Prakash *et al*. [19, 20] have presented a

comparative study between the experiment of visualization, the measurements by LDV and the CFD simulation of a round jet flowing in a cylindrical cavity with a porous layer. Graminho and De Lemos [21] have examined the influence of the presence of a porous layer at the bottom of a hot cavity cooled by a turbulent round jet. Benaissa [22] and Kendil *et al.* [23] have achieved an experimental and a numerical study of a turbulent axisymmetric round jet flowing inside a cylindrical cavity open upstream, for Reynolds numbers ranging between 22,000 and 50,000. The distance between the jet exit and the cavity bottom, L_f is varied from 2 to 30 jet diameters. The flow velocity field was measured using hot wire anemometry. The computations were achieved using the standard k-ε model combined to the wall functions. Chandratilleke *et al*. [24] have proposed a new technique for improving the cooling of a hot surface by a coaxial jet directed to the surface of a cylindrical cavity. Voropayev *et al.* [25] have realized an experimental study of a turbulent round jet located in a long cylinder for the applications to crude-oil storage tanks for strategic petroleum U.S.

In the present paper, the case of a round jet impinging perpendicularly a hot cylindrical cavity is investigated numerically using the Reynolds stress model (RSM) coupled to the logarithmic wall function for the wall treatment. The jet exits from a long horizontal pipe in a cylindrical hot cavity. The radius of the pipe and the cavity are R_{jet} and R_{cav}, respectively. The configuration is sketched in fig. 1. For the validation, the flow field are compared to the measurements of Benaissa [22] for the case $L_f = 8d$. The purpose of this paper is to investigate the thermal study and to examine the phenomenon for different values of the impinging distance ($4 \le L_f \le 35$).

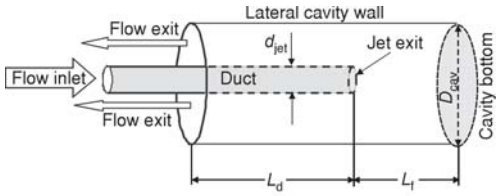

Figure 1. Geometry and computational domain

Numerical modeling and computational methodology

Modeling of flow filed and heat transfer

The flow is assumed steady in average, turbulent, and axisymmetric. The fluid is incompressible with constant thermo physical properties. The steady Reynolds average Navier Stokes (SRANS) equations coupled to the averaged energy equation of the turbulent compressible flows are written as:

– the mass equation

$$\frac{\partial U_i}{\partial x_i} = 0 \tag{1}$$

– the momentum equation

The Reynolds averaged momentum are:

$$\frac{\partial(\rho U_i U_j)}{\partial x_i} - \frac{\partial}{\partial x_i}\left[\mu\left(\frac{\partial U_i}{\partial x_j} + \frac{\partial U_j}{\partial x_i}\right)\right] = -\frac{\partial}{\partial x_i}\left(P + \frac{2}{3}\mu\frac{\partial U_k}{\partial x_k}\right) - \frac{\partial}{\partial x_i}(\rho\overline{u_i u_j}) + S_{Mi} \tag{2}$$

where P is the static pressure and S_{Mi} – the sum of body forces. This equation is coupled to second order RSM turbulence model. Second order models are based on transport equations for every component of the Reynolds stress tensor and the dissipation rate. These models do not use the eddy viscosity hypothesis, but solve an equation for the transport of Reynolds stresses. Algebraic Reynolds stress models solve algebraic equations for the Reynolds stresses [26], whereas

differential Reynolds stress models solve differential transport equations individually for each Reynolds stress component. The exact production term and the inherent modeling of stress anisotropies theoretically make Reynolds stress models more suited to complex flows. In the differential stress model, a separate transport equation must be solved for each of the six Reynolds stress components of $\rho\overline{u_i u_j}$.The standard Reynolds stress model is based on dissipation ε equation:

$$\frac{\partial}{\partial x_i}(\rho U_k \overline{u_i u_j}) - \frac{\partial}{\partial x_k}\left[\left(\mu\delta_{kl} + C_s\rho\frac{k}{\varepsilon}\right)\frac{\partial(\overline{u_i u_j})}{\partial x_l}\right] = P_{ij} - \frac{2}{3}\delta_{ij}\rho\varepsilon + \Phi_{ij} \tag{3}$$

where P_{ij}, the production term, is given by:

$$P_{ij} = \rho\overline{u_i u_k}\frac{\partial U_j}{\partial x_k} - \rho\overline{u_i u_k}\frac{\partial U_i}{\partial x_k} \tag{4}$$

and Φ_{ij} is the pressure strain correlation. This term can be separated into two parts:

$$\Phi_{ij} = \Phi_{ij,1} + \Phi_{ij,2} \tag{5}$$

where $\Phi_{ij,1}$ is the "slow" term, also known as the return-to-isotropy term, and $\Phi_{ij,2}$ is called the "rapid" term.

As the turbulence, dissipation appears in the individual stress equations, an equation for ε is then required. This later is given by:

$$\frac{\partial(\rho\varepsilon)}{\partial t} + \frac{\partial(\rho U_k\varepsilon)}{\partial x_k} = \frac{\varepsilon}{k}(C_{\varepsilon 1}P_k - C_{\varepsilon 2}\rho\varepsilon + C_{\varepsilon 1}P_{\varepsilon b}) + \frac{\partial}{\partial x_k}\left[\left(\mu\delta_{kl} + C_\varepsilon\rho\frac{\varepsilon}{k}\overline{u_k u_l}\right)\frac{\partial\varepsilon}{\partial x_l}\right] \tag{6}$$

There are three version of the standard Reynolds stress models based on the ε-equation developed by Launder *et al.* [26]. These are called as LRR-IP, LRR-QI, and SSG. For the LRR-IP and LRR-QI models, the pressure-strain correlation is linear; "IP" stands for isotropization of production and is the simplest of the three models. The SSG model was developed by Speziale, *et al.* [27] uses a quadratic relation for the pressure-strain correlation. The pressure-strain correlations have a following form depending on the anisotropy tensor a_{ij}, the mean strain rate tensor S_{ij} and vorticity tensor Ω_{ij}.

$$\Phi_{ij,1} = -\rho\varepsilon\left[C_{S1}a_{ij} + C_{S2}\left(a_{ik}a_{kj} - \frac{1}{3}a_{mn}a_{mn}\delta_{ij}\right)\right] \tag{7}$$

$$\Phi_{ij,2} = -C_{r1}Pa_{ij} + C_{r2}\rho k S_{ij} + C_{r3}\rho k S_{ij}\sqrt{a_{mn}a_{mn}} + $$
$$+ C_{r4}\rho k\left(a_{ik}S_{jk} + a_{jk}S_{ik} - \frac{2}{3}a_{kl}S_{kl}\delta_{ij}\right) + C_{r5}\rho k(a_{ik}\Omega_{jk} + a_{jk}\Omega_{jk}) \tag{8}$$

where

$$a_{ij} = \frac{\overline{u_i u_j}}{k} - \frac{2}{3}\delta_{ij}, \quad S_{ij} = \frac{1}{2}\left(\frac{\partial u_i}{\partial x_j} + \frac{\partial u_j}{\partial x_i}\right), \quad \Omega_{ij} = \frac{1}{2}\left(\frac{\partial u_i}{\partial x_j} + \frac{\partial u_j}{\partial x_i}\right)$$

The production due to the buoyancy is neglected in this study.

– the energy equation

$$\frac{\partial T}{\partial t} + U_i\frac{\partial T}{\partial x_i} = \frac{\partial}{\partial x_i}\left(a\frac{\partial T}{\partial x_i} - \overline{u_i\theta}\right) \quad \text{where} \quad -\rho\overline{u_i\theta} = \alpha_t\frac{\partial T}{\partial x_i} \tag{9}$$

By analogy with molecular transport, the turbulent Prandtl number for energy transport equation can be deduced by:

$$\alpha_t = \frac{\nu_t}{\mathrm{Pr}_t} \tag{10}$$

The model constants are listed in tab. 1.

Table 1. Reynolds stress constant model

$C_{\varepsilon 1}$	$C_{\varepsilon 2}$	C_{μ}	C_{s1}	C_{s2}	C_{r1}	C_{r2}	C_{r3}	C_{r4}	C_{r5}	$\mathrm{Pr_t}$
1.44	1.92	0.09	1.7	–1.05	0.9	0.8	0.65	0.625	0.2	0.85

Wall function approach

The wall treatment boundary conditions were achieved using the wall function technique of Launder and Spalding [28] that combine the viscosity affected region (viscous sub-layer) between the wall and the fully turbulent region, and were most widely used for industrial flows. Reynolds analogy between momentum and energy transport equation gives a similar logarithmic law for mean temperature.

The dimensionless variables of distance and velocity are defined as:

$$U_p^+ = \frac{U_p}{U_\tau}; \quad y_p^+ = \frac{\partial U_\tau y_p}{\mu} \quad \text{where} \quad U_\tau = \sqrt{\frac{\tau_p}{\rho}} \quad \text{and} \quad \tau_p = \rho \frac{\sqrt[4]{C_p}\sqrt{k_p}U_p}{U_p^+}$$

The index p means the value at the first point of grid close to the wall.

In the case of impinging jets, it is recommended to use near the wall the non-equilibrium wall function proposed by Kim and Choudhury [29].

Geometry and boundary conditions

The jet exit velocity is imposed to a given Reynolds numbers. The length of the pipe is of 24 nozzle diameter ($L_\mathrm{d} = 24d$) for all configurations in order to obtain the fully developed flow at the exit. The nozzle diameter d is of 3.7 cm. The cavity radius R_cav is of $3.92d$. Tridimensional computations were achieved over the half of the configuration domain in order to spare calculation time. Four types boundaries conditions are imposed.

Air jet exit: The conditions at the duct inlet boundary are important in predicting the centerline velocity and shear stress. Constant values were considered for this boundary, as:

$$U = U_0, \quad V = 0, \quad T = T_0, \quad k_{in} = IU_0^2 \quad \text{and} \quad \varepsilon_{in} = \frac{k_{in}^{1.5}}{0.15d} \quad \text{where} \quad I = 10^{-4}$$

The wall boundary: The velocity components are set to zero for each wall .Constant temperature $T_\mathrm{w} > T_0$ was imposed for each cavity walls and the duct wall is considered adiabatic.

Air exit boundary: The OUTFLOW (fully developed) boundary conditions were used. Constant relative static pressure kept at atmospheric level at this boundary was imposed;

The symmetry: This boundary condition is imposed in (y- z) plane ($x = 0$) (fig. 2). The perpendicular velocity and Reynolds stresses components and the gradient of the all other dependent variables are set to zero.

Modeling parameters

The numerical thermal and flow control parameters used in this study are summarized in tab. 2. The validation was achieved according to experiments data for the case $L_\mathrm{f} = 8d$. The numerical predictions were performed in order to investigate the effect of the impinging distance L_f on the flow structure and heat transfer.

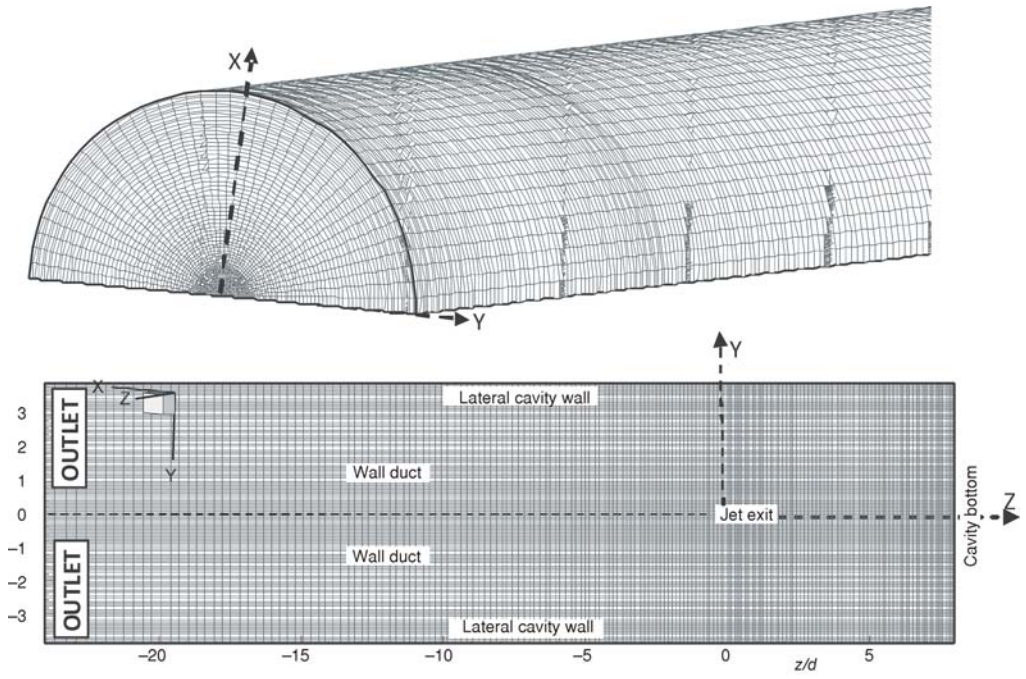

Figure 2. Geometry and a typical mesh ($L_f = 8d$) 3-D view and symmetry plane

Table 2.The flow control parameters

R_{cav}	d	L_d	L_f	Re	T_0	T_w
14.5 cm	3.7 cm	$24d$	$2d \le L_f \le 30d$	$2 \cdot 10^4 \le Re \le 1 \cdot 10^5$	300 K	360 K

The equations for the mean and turbulent quantities are transformed by transport equations composed of convection, diffusion and source terms. They are discretized using finite volume technique on collocated non-uniform meshes. The convection and diffusion terms were discredited by means of POWER LAW schemes for all variables (U, V, T, k, $\overline{u_i u_j}$, and ε); while for the pressure the second-order scheme was used. The pressure velocity coupling is achieved using SIMPLEC algorithm. Usually, the source terms of all equations are linearized to insure the stability of the solution. The non-uniform structured grids were used. Refinements before and after the nozzle exit were managed in order to describe the entrainment accurately. Sufficiently fine grids were used near the cavity and duct walls to predict very high gradient of variables prevailed in the viscous sub-layer (fig. 2). The uncertainties in numerical results were evaluated by checking the convergence through mesh refinement calculations. Calculations show that for example for the case $L_f = 8d$ (tab. 3); the number of nodes used in case (c) were adequate, since no difference was noted when compared with case (d). Further mesh refinement and numerical tests were carried out to check the stability of the solution

Table 3. Different grids ($L_f = 8d$)

Test	(a)	(b)	(c)	(d)
Nodes	231557	350003	454217	558886

Results and discussion

Dynamic field

The present work has described the behavior of a confined jet impinging a heated cylindrical cavity. Both, the velocity and the thermal fields are investigated to evidence the effect of the jet interaction on the cavity. The numerical simulations were carried out for Reynolds number ranges from $2 \cdot 10^4$ to 10^5 and different impinging distances (jet exit nozzle-cavity bottom L_f) ranging from $2d$ to $30d$. For the validation, the reduced axial velocity prediction was compared to experimental values of Tani and Komatsu [30] determined on behalf of the same conditions (fig. 3). Good agreement with the experiment is obtained for three impinging distances L_f($L_f = 4d$, $L_f = 8d$, and $L_f = 12d$).

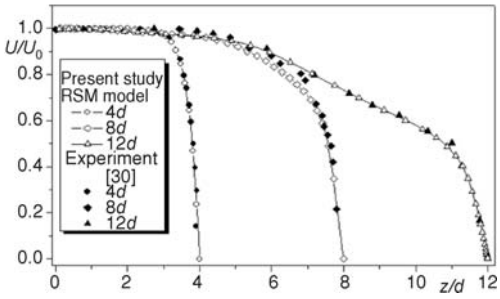

Figure 3. Reduced axial velocity profile along the jet axis

The evolution of the axial component of the velocity vector (fig. 4) was compared to its corresponding experimental values of Benaissa [22] for the case $L_f = 8d$. Four cross-sections of the cavity were considered: $z/d = 0.08$, 1.89, 4.06, and 6.48. It is noticed that the numerical predictions are in good agreement with the experimental data. The evolution of the Reynolds shear stress $\overline{uv}$ and u^2 according to the reduced radial distance η are also compared to corre-

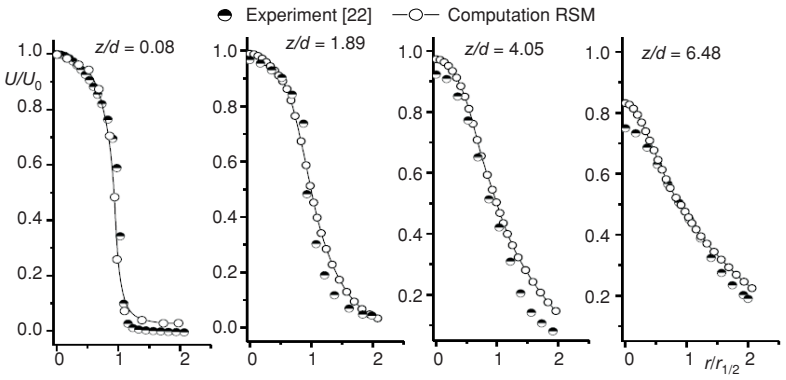

Figure 4. Radial evolution of the axial velocity at different downstream sections $L_f = 8d$

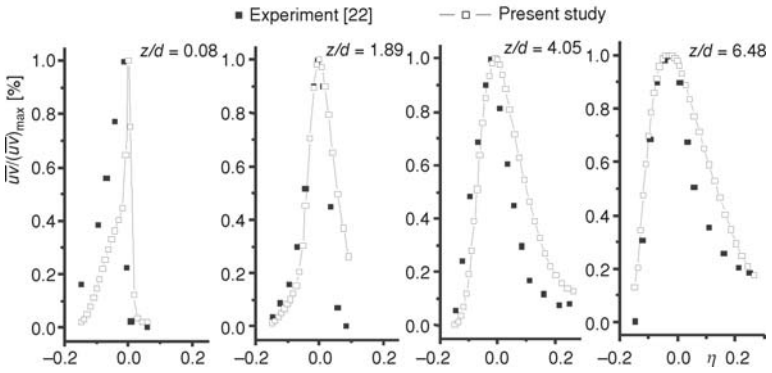

Figure 5. Radial evolution of component of Reynolds stress at different cross-sections $L_f = 8d$ and Re = 37400

sponding experimental data of Benaissa, [22] (figs. 5 and 6). Maximum value are reached around $\eta = 0$. These first comparisons indicate that the simulation for the case $L_f = 8d$ will predicts well this flow. Minor discrepancies are observed between the two predictions in the areas of reverse flow, which are caused by hot-wire measurements that are not re-commended for re-circulated flow.

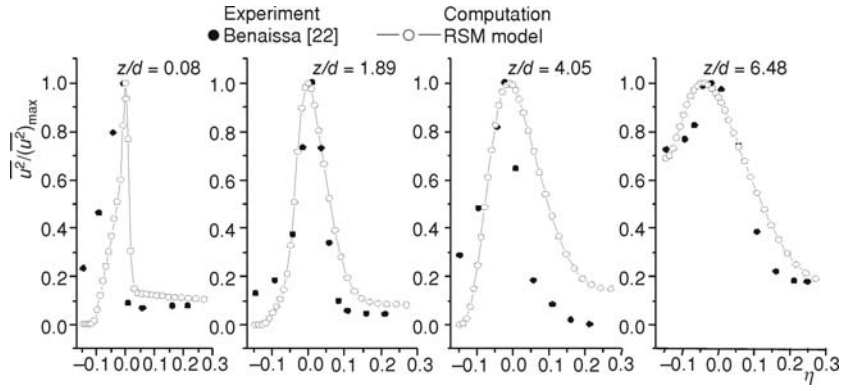

Figure 6. Radial evolution of component of Reynolds stress for several cross-sections $L_f = 8d$ and Re = 37400

The influence of the impinging distance L_f on the flow structure interaction is described by the magnitude of the vorticity contours computed using the Reynolds stress model (fig. 7). The contours plots show that the interaction of the jet into the cavity produces two deterministic eddies on each side of the jet with opposite swirl. For short impinging distances $2d \leq L_f \leq 8d$, the jet impinges the cavity bottom and returns towards the exit of the cavity. The reverse flow is then split into two parts:

– the outflow which leaves the cavity at low velocity in the opposite direction of the jet, and
– an entrained flow is sucked by the jet, leads the formation of a stable toroidal eddy near the cavity bottom. This zone is characterized by a weak mean velocity, high turbulence energy and a negative pressure due to the Coanda effect [11, 12].

The principal jet is also narrowed. For $L_f \leq 4d$, the center of this eddy remained identical for several impinging distance. The case of $L_f = 8d$ is in good agreement with experimental visualisation of Benaissa [22]. For $L_f = 20d$, appears close to the cavity bottom wall a secondary toroidal vortex which increases in volume when L_f increases. The size of the first vortex remains constant for $8d \leq L_f \leq 35d$.The size of the first vortex remains constant. The space between this later and the cavity bottom is a seat for the generation of secondary eddies. For very large impinging distance $L_f \leq 24d$, third contra rotating toroidal eddy (swirl) appears in the corner of the cavity, this swirl becomes more obvious and larger when the impinging distance increases $L_f \leq 30d$. The maximum values of vorticity are attained around the jet exit area. The Reynolds number does not have any influence on the global structure of the vorticity, it has only an effect on the magnitude as expected.

Figure 8 shows the influence of the impinging distance L_f on the axial velocity profiles across several perpendicular sections (ξ: 0.01, 0.25, 0.5 and 0.8) at Re = 37400. For several impinging distance, the reverse flow was evidenced by negative values of axial velocity near the lateral cavity wall.

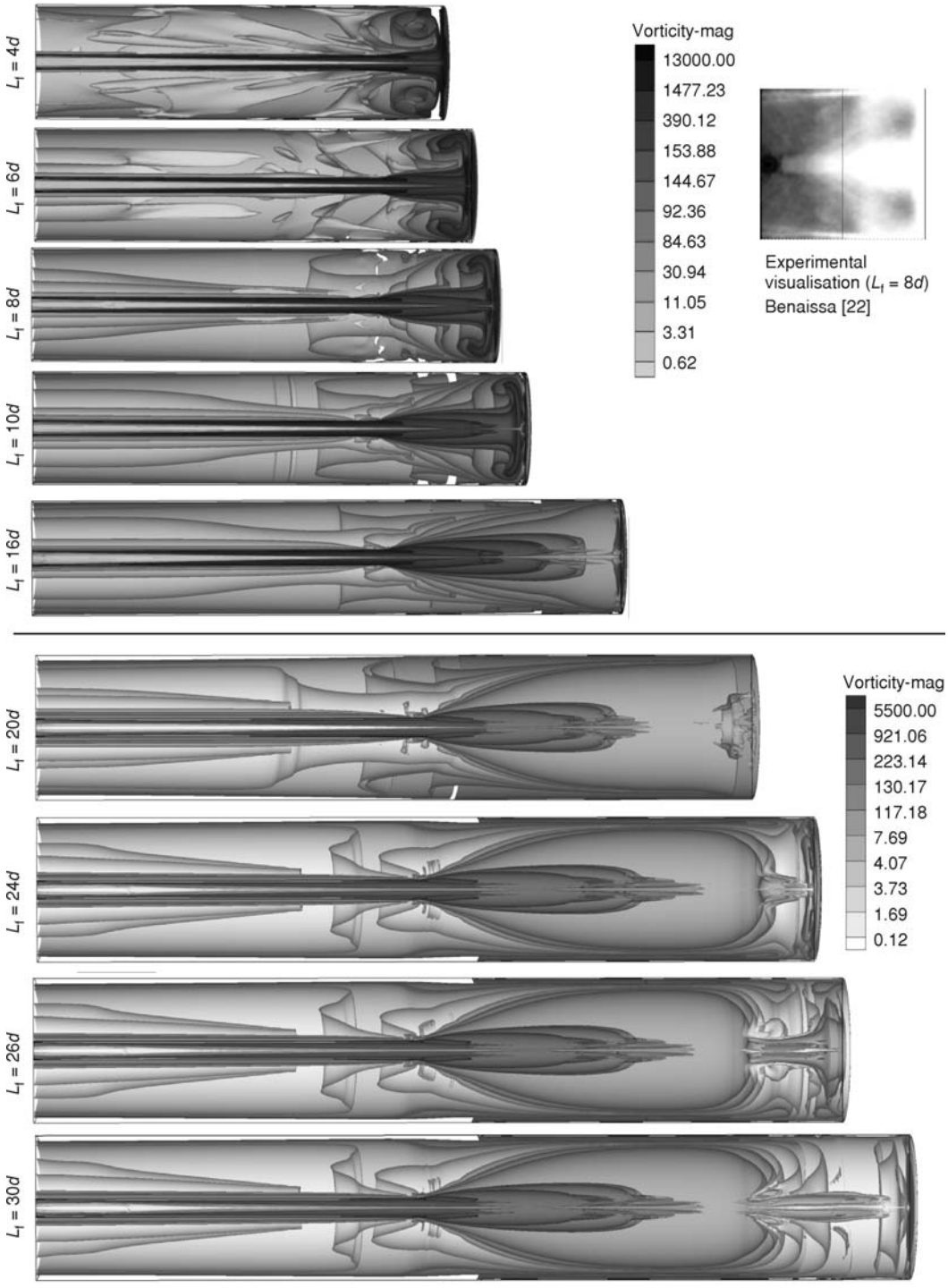

Figure 7. Effect of the impinging distance L_f on vorticity magnitude in s^{-1} (Re = 37400)

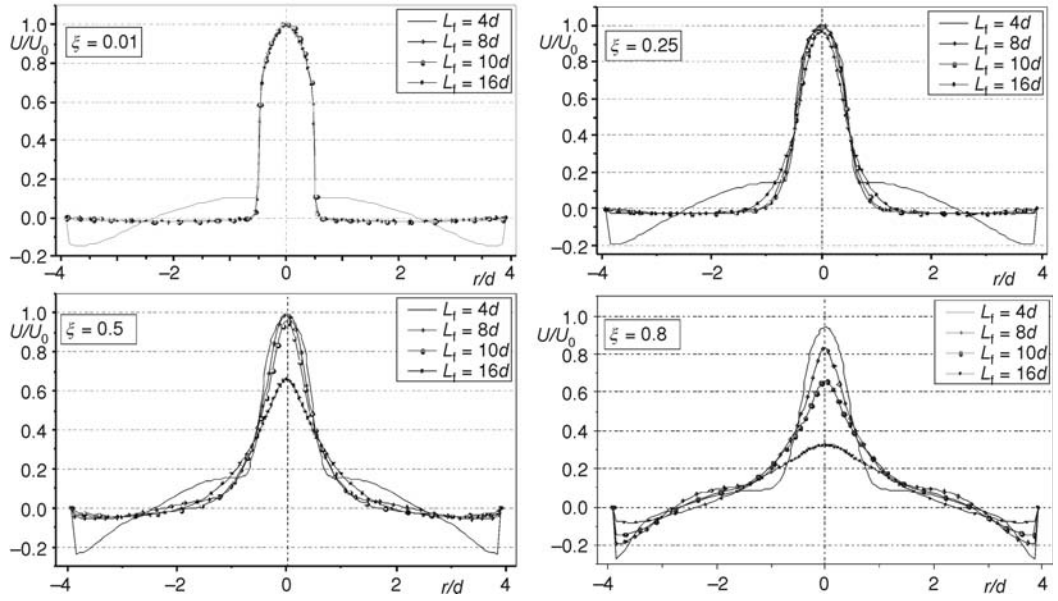

Figure 8. Effect of the impinging distance L_f on axial velocity (Re = 37400)

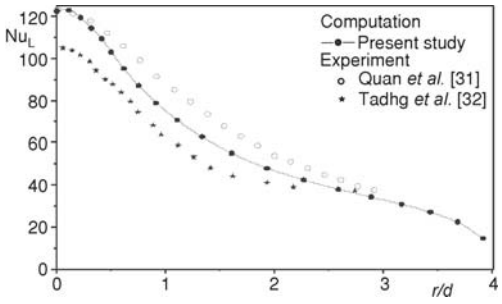

Figure 9. Local Nusselt number on the cavity bottom

Thermal study

For the thermal study, the effects of the impinging distance L_f and Reynolds number on the local Nusselt number Nu_L, were investigated. The local Nusselt number is examined for the two cavity walls (bottom face and lateral face).

In order to validate the numerical method for heat transfer predictions, comparisons were performed with experiment data of Quan, [31] and O'Donovan and Murray [32] of the case of a round jet impinging perpendicularly a hot wall. A good agreement is obtained qualitatively with the experiment (fig. 9). Minor differences are noticeable between the curve shapes, which can be explained by the effect of confinement of lateral cavity wall.

Figures 10(a) and (b) illustrate, respectively, the local Nusselt number evolution along the cavity bottom walls and cavity lateral, according to the Reynolds number, for the case $L = 8d$. The visual analysis of these two figures shows that the increase in the Reynolds number led to the increase of the heat transfer. This evolution is completely predictable since the increase of Reynolds number, hence enhances the heat transfer. Particularly on the bottom cavity wall, optimal and minimum Nusselt number values corresponding to stagnation and re-attachment points, respectively. The influence of the impinging distance was evidenced through temperature profiles (fig. 11). For big impinging distance ($L_f = 16d$), a homogeneous heating of flow is obtained. Minimum temperature values are observed at jet exit and maximal values are reached at lateral cavity wall.

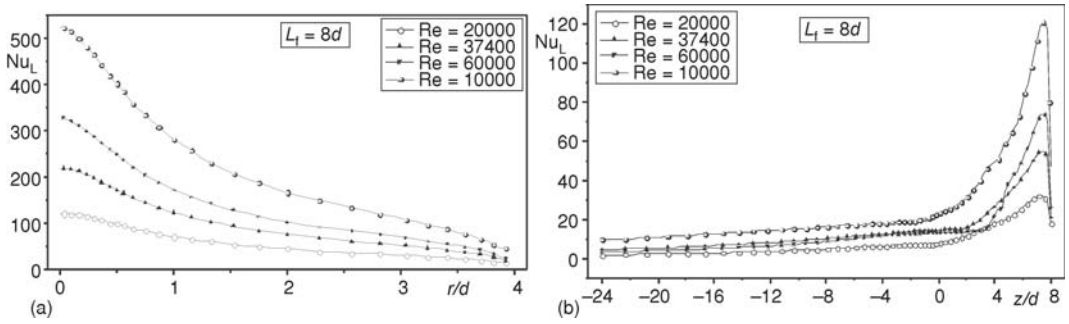

Figure 10. Effect of Reynolds number on Nusselt number ($L_f = 8d$)

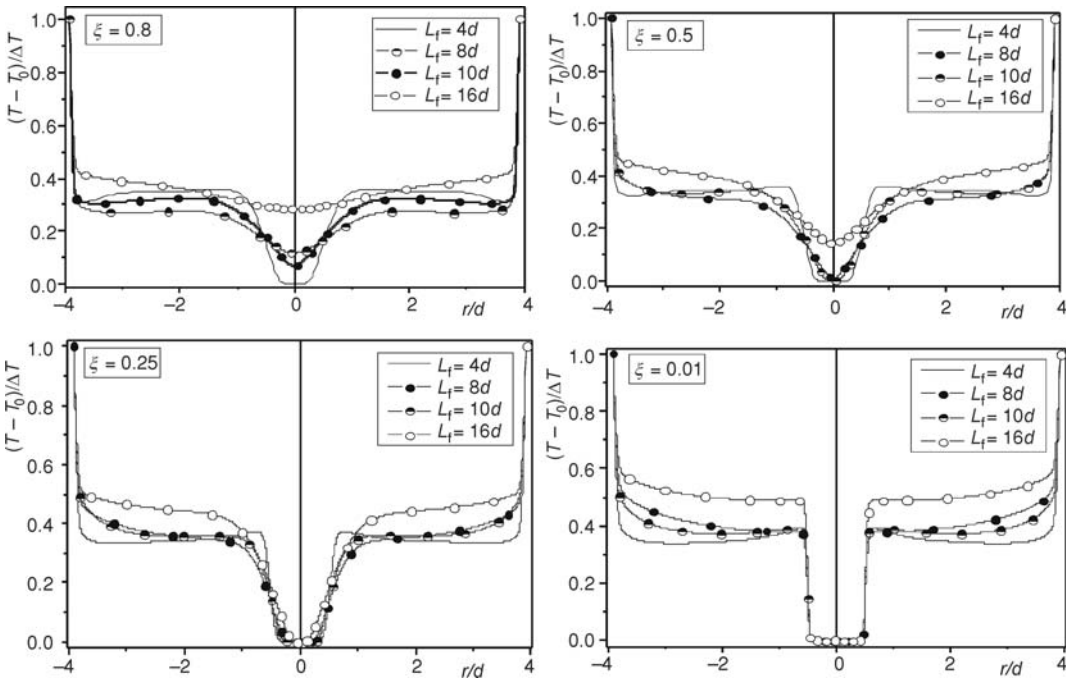

Figure 11. Effect of the impinging distance L_f on temperature (Re = 37400)

Figure12 shows the effect of the impinging distance on local Nusselt number along each cavity wall. The first peak (maximum Nusselt number) corresponds to the stagnation point and decrease to $r = 0.5d$ matching to the section jet this maximum is due to the existence of a quasi-uniform velocity profile around the stagnation point. For a largest impinging distance, this maximum disappears caused by secondary eddies located in the cavity bottom region, creating an air cushion preventing the cooling of the cavity hot walls by the jet (see fig. 7).

Finally, the numerical results of the average Nusselt numbers evolution according to the impinging distance, fig. 13, was expressed for a several Reynolds numbers by the following correlation:

$$\overline{\mathrm{Nu}} = 4.6017 + 10^{-3}(7.98 - 0.3123L_f)\,\mathrm{Re}^{0.883}$$

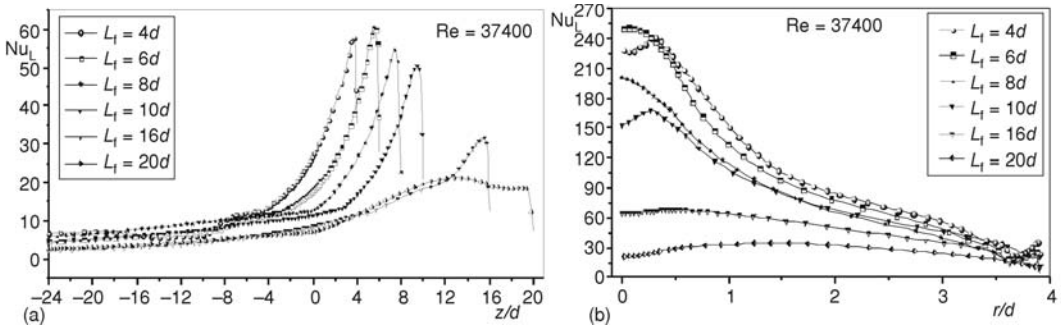

Figure 12. Effect of impinging distance on local Nusselt number (Re= 37400); (a) side wall, (b) bottom wall

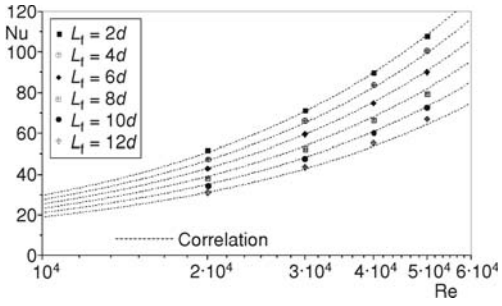

Figure 13. Effect of impinging distance on mean Nusselt number (Re= 37400)

This correlation is valid for $L_f \leq 12d$. The case of large impinging distance ($L_f > 12d$), induce secondary eddies in the cavity bottom area, which do not characterise heat transfer of jet to wall impingement

Conclusions

The interaction of turbulent axisymmetric jet issuing into a cylindrical hot cavity was investigated numerically using Reynolds stress turbulence model. A parametric study was conducted by varying the impinging distance for several Reynolds numbers. The fluid structure was determined for different impinging distances.

- The flow is turbulent and steady in average as confirmed by previous study of the same configuration.
- The flow structure was independent of the Reynolds number (turbulent).
- The velocity profiles agree with experimental data for the case $L_f = 4d$, $8d$, and $12d$.
- A reverse flow occurs within the cavity corner and near the cavity bottom. It interacted with the main flow producing a toroidal swirl close to the jet exit.

The increase of Reynolds number enhances the heat transfer. The results are compared with an experimental available case of a jet, impinging normally onto a flat plate. It is found, that for large impinging distance, two secondary vortices weaken the heat transfer. This weakening is due to the existence of the secondary eddies in the cavity bottom area. The computed heat transfer data are believed to be in good agreement with previous works. However, the experimental verification of the results is strongly recommended and will be performed in the future. The evolution of average Nusselt number is correlated according to the impinging distance and Reynolds number $\overline{\mathrm{Nu}} = f(L_f, \mathrm{Re})$.

Nomenclature

a – thermal diffusivity, [m^{2}s^{-1}]
d – jet exit diameter, [m]
k – kinetic energy of turbulence, [m^{2}s^{-2}]
L_d – length of the pipe, [m]
L_f – distances jet exit nozzle-cavity bottom, [m]
$\overline{\mathrm{Nu}}$ – average Nusselt number [$= \int_0^{R_{cav}} (2\pi r \mathrm{Nu})\mathrm{d}r/\pi(R_{cav})^2$], [–]
Nu_L – local Nusselt number ($= q_w d/\lambda\Delta T$), [–]
P – mean pressure, [Pa]
q_w – heat flux per unit area, [Wm^{-2}]

Re – Reynolds number (= $U_i d_{jet}/\nu$), [–]
R_{cav} – cavity radius, [m]
R_{jet} – jet exit radius, [m]
$r_{1/2}$ – radial position corresponding to $U_{max}/2$, [m]
T – temperature, [K]
U_0 – jet inlet velocity, [ms^{-1}]
U^+ – non-dimensional velocity, [–]
U, V – velocity components, [ms^{-1}]
U_{max} – maximum mean velocity, [ms^{-1}]
$\overline{u_i u_j}$ – Reynolds stress component, [m^{2}s^{-2}]
y^+ – non-dimensional distance, [–]

Greek symbols

ε – dissipation rate of turbulent energy, [m^{2}s^{-3}]
η – dimensionless axial distance (= $(r - R_{jet})/(R_{cav} - R_{jet})$), [–]
θ – fluctuating temperature, [K]
I – turbulence intensity, [–]
λ – thermal conductivity of air, [Wm^{-2}K^{-1}]
ν – kinematic molecular viscosity, [m^{2}s^{-1}]
ν_t – kinematic turbulent viscosity, [m^{2}s^{-1}]
ξ – dimensionless axial distance (= $(z - L_d)/ L_f$)
ρ – air density, [kgm^{-3}]

Reference

[1] Polat, S., *et al.*, Numerical Flow and Heat Transfer under Impinging Jets, *Annual Review of Numerical Fluid Mechanics and Heat Transfer, 2* (1989), 2, pp. 157-197
[2] Gilard, V., Brizzi, L. E., Slot Jet Impinging a Curved Wall, *Journal of Fluids Engineering, 127* (2005), 3, pp. 595-603
[3] Gilard, V., Brizzi, L. E., Study of a Line of Jes Impacting a Concave Wall by Stereoscopic PIV (in French), *Comptes Rendus Mecanique, 334* (2006), 1, pp. 74-82
[4] Choi, M., *et al.*, Measurements of Impinging Jet Flow and Heat Transfer on a Semi-Circular Concave Surface, *International Journal of Heat and Mass Transfer, 43* (2000), 10, pp. 1811-1822
[5] Shuja, S. Z., *et al*., Jet Impingement on Cylindrical Cavity: Conical Nozzle Considerations, *Journal of Fluids and Structures, 23* (2007), 7, pp. 1106-1118
[6] Shuja, S. Z., *et al*., Flow Emerging from Annular-Conical Nozzle Combinations and Impinging onto a Cylindrical Cavity, *International Journal of Thermal Sciences, 48* (2009), 5, pp. 975-984
[7] Shuja, S. Z., *et al*., Jet Impingement onto a Conical Cavity: Effects of Annular Nozzle Outer Angle and Jet Velocity on Heat Transfer and Skin Friction, *International Journal of Thermal Sciences, 48* (2009), 5, pp. 985-997
[8] Terekhov, V. I., *et al*., Impingement of an Impact Jet onto a Spherical Cavity, Flow Structure and Heat Transfer, *International Journal of Heat and Mass Transfer, 52* (2009), 11, pp. 2498-2506
[9] Colucci, D. W., Viskanta, R., Effect of Nozzle Geometry on Local Convective Heat Transfer to a Confined Impinging Air Jet, *Experimental Thermal and Fluid Science, 13* (1996), 1, pp. 71-80
[10] Jeng, T.-M., Tzeng, S.-C., Numerical Study of Confined Slot Jet Impinging on Porous Metallic Foam Heat Sink, *International Journal of Heat and Mass Transfer, 48* (2005), 23, pp. 4685-4694
[11] Mataoui, A., *et al*., Flow Regimes of Interaction of a Turbulent Plane Jet into a Rectangular Cavity: Experimental Approach and Numerical Modelling, Flow, *Turbulence and Combustion, 67* (2001), 4, pp. 267-304
[12] Mataoui, A. Schiestel, R., Unsteady Phenomena of an Oscillating Turbulent Jet Flow Insidea Cavity:Effect of Aspect Ratio, *Journal of Fluids and Structures, 25* (2009), 1, pp. 60-79
[13] Jaramillo, J. E., *et al*., DNS and RANS Modeling of a Turbulent Plane Impinging Jet, *International Journal of Heat and Mass Transfer, 55* (2012), 4, pp. 789-801
[14] Lawsona, N. J., *et al*., Control of a Submerged Jet in a thin Rectangular Cavity, *Journal of Fluids and Structures, 20* (2005), 8, pp. 1025-1042
[15] Schwarze, R., *et al*., Experimental and Numerical Investigations of a Turbulent Round Jet into a Cavity, *Inter Journal of Heat and Fluid Flow, 29* (2008), 6, pp. 1688-1698
[16] Kang, H., Tao, W., Heat and Mass Transfer for Jet Impingement in a Cylindrical Cavity with One End Open to the Ambiant Air, AIAA paper 89-0173, 1989
[17] Risso, F., Fabre, J., Diffusive Turbulence in a Confined Jet Experiment, *J. Fluid Mech., 337* (1997), pp. 233-261
[18] Baydar, E., Ozmen,Y., An Experimental and Numerical Investigation on a Confined Impinging Air Jet at High Reynolds Numbers, *Applied Thermal Engineering, 25* (2005), 2, pp. 409-421

[19] Prakasha, M., *et al*., Impinging Round Jet Studies in a Cylindrical Enclosure With and without a Porous Layer: Part I – Flow Visualisations and Simulations, *Chemical Engineering Science, 56* (2001), 12, pp. 3855-3878
[20] Prakasha, M., *et al*., Impinging Round Jet Studies in a Cylindrical Enclosure with and without a Porous Layer: Part II – LDV Measurements and Simulations, *Chemical Engineering Science, 56* (2001), 12, pp. 3879-3892
[21] De Lemos, M. J. S., *et al.*, Simulation of Turbulent Impinging Jet into a Layer of Porous Material Using a Two-Energy Equation Model, *Numerical Heat Transfer, Part A: Applications, 59* (2011), 10, pp. 769-798
[22] Benaissa, A., Contribution to the Study of the Evolution of the Axial Symmetric Air Jet in a Cylindrical Cavity (in French), M. Sc. thesis, *Fluid Mechanics*, USTHB, Alger, Algeria, 1985
[23] Kendil, F. Z., *et al*., Flow Structures of a Round Jet Evolving into a Cylindrical Cavity, *International Journal of Transport Phenomena, 11* (2009), 2, pp. 165-183
[24] Chandratilleke, T. T., *et al*., Heat Transfer and Flow Characteristics of Fluid Jets Impinging on a Surface with Cavities, *Journal of Enhanced Heat Transfer, 17* (2010), 3, pp. 223-229
[25] Voropayev, S. I., *et al*., Evolution of a Confined Turbulent Jet in a Long Cylindrical Cavity: Homogeneous Fluids, *Physics of Fluids, 23* (2011), 11, pp. 115106
[26] Launder, B. E., *et al*., Progress in the Developments of a Reynolds-Stress Turbulence Closure, *J. Fluid Mechanics, 68* (1975), 3, pp.537-566
[27] Speziale, C. G., *et al*., Modeling the Pressure-Strain Correlation of Turbulence: an Invariant Dynamical Systems Approach, *J. Fluid Mechanics, 277* (1991), pp. 245-272
[28] Launder, B. E., Spalding, D. B., The Numerical of Computation of Turbulent Flow, *Computer Methods in Applied Mechanics and Engineering, 3* (1974), 2, pp. 269-289
[29] Kim, S. E., Choudhury, D., A Near-Wall Treatment Using Wall Functions Sensitized to Pressure Gradient, *ASME FED, 217* (1995), *Separated and Complex Flows*
[30] Tani, I., Komatsu, Y., *Impingement of a Round Jet on a Flat Surface*, The International Congress of Applied Mechanics, Munich, Germany Springer, Berlin, 1966, pp. 672-676
[31] Quan, L., Study of Heat Transfer Characteristics of Impinging Air Jet Using Pressure and Temperature Sensitive Luminescent Paint, Ph. D. thesis, University of Central Florida, Fla., USA, 2006
[32] O'Donovan, T. S., Murray, D. B., Jet Impingement Heat Transfer – Part I: Mean and Root-Mean-Square Heat Transfer and Velocity Distributions, *International Journal of Heat and Mass Transfer, 50* (2007), 17-18, pp. 3291-3301

Paper submitted: October 1, 2012
Paper revised: June 12, 2013
paper accepted: June 21, 2013